Estimating inland water quality parameters using Wyvern Dragonette-001 hyperspectral imagery, a case study from the St. Lawrence River, Canada

Mohsen Ansari [1], Anders Knudby [1]

[1] Department of Geography, Environment and Geomatics, University of Ottawa, 75 Laurier Avenue East, Ottawa, ON, K1N 6N5, Canada – mohsen.ansari@uottawa.ca, aknudby@uottawa.ca

Keywords: Hyperspectral Imagery, Wyvern Dragonette, Water Quality, Machine Learning, Inland Water, Remote Sensing.

Abstract

This study evaluates the feasibility of using Wyvern Dragonette-001 hyperspectral imagery for retrieving inland Water Quality Parameters (WQPs), turbidity, Suspended Sediments (SS), and Dissolved Organic Carbon (DOC), in a section of the St. Lawrence River, Québec, Canada. Two field campaigns were conducted on 2 August and 6 September 2024, providing in-situ measurements for model development and validation. Water-leaving reflectance (ρ_w) was derived using ACOLITE, and a spatial blocking approach was applied to reduce spatial autocorrelation between training and testing datasets. Random Forest (RF) models were trained with hyperparameter tuning using Optuna and 5-fold cross-validation. Results show good performance for turbidity estimation (R^2 = 0.91), while SS and DOC exhibited lower accuracy in compared to turbidity, partly due to limited sample sizes. Feature importance analysis indicated that green bands were most relevant for DOC, near-infrared (NIR) bands for SS, and red bands for turbidity. Elevated ρ_w values in NIR bands suggest potential influences from adjacency effects, atmospheric correction limitations, or sensor characteristics. Overall, Dragonette-001 demonstrates capability for turbidity mapping, while improvements in spectral coverage, atmospheric correction, and in-situ data availability are needed for accurate retrieval of DOC and SS.

1. Introduction

Monitoring inland WQPs is essential for managing freshwater ecosystems and assessing anthropogenic impacts (Mishra et al., 2017). Satellite remote sensing provides a cost-effective and large-scale approach for monitoring inland WQPs (IOCCG, 2000). However, most existing satellite sensors have limited spectral resolution, restricting their ability to capture subtle optical variations expressed by inland WQPs, and/or insufficient spatial resolution to yield valid water-only pixels in narrow rivers or nearshore zones (Ansari et al., 2025a).

Recent advances in hyperspectral satellite technology have created new opportunities for inland WQP monitoring. The Wyvern Dragonette-001, launched in April 2023, provides hyperspectral imagery with a spatial resolution of 5.3 m and 23 spectral bands within the visible to NIR range (503-799 nm) (Ansari et al., 2025a; Wyvern Dragonette, 2023). Given its novelty, the potential of such imagery for assessing WQPs in inland water remains largely unexplored. A recent review (Ansari et al., 2025a) evaluating the sensor's spectral resolution and signal-to-noise ratio for retrieving inland WQPs indicated that Dragonette-001 is suitable for estimating non-algal particles and shows potential for chlorophyll-*a* mapping, although it is likely unsuitable for retrieving Colored Dissolved Organic Matter (CDOM).

This study reports on a practical test that assessed the feasibility of using Wyvern Dragonette-001 imagery to retrieve turbidity and SS, which are optically active, as well as DOC, an non-optically active parameter (which does not directly affect the attenuation of light in water (Gholizadeh et al., 2016; Tesfaye, 2024)), in a portion of the St. Lawrence River, Québec, Canada.

2. Study Area and Data

The study area covers ~100 km² of the St. Lawrence River, north of Montréal, near the proposed Contrecoeur Terminal expansion (Figure 1). Two field campaigns were conducted on 2 August and 6 September 2024, synchronized with Dragonette-001 overpasses. A total of 12,236 in-situ turbidity measurements (in NTU) were collected using a YSI multiparameter sonde operated by WSP Canada Inc. Additionally, 21 water samples were collected and analyzed in the laboratory for SS and DOC (in mg/L), including duplicate measurements at a randomly selected location, resulting in 21 samples from 19 distinct sites to assess laboratory accuracy. All field measurements were georeferenced with a Trimble R1 GNSS receiver to ensure sub-meter positional accuracy.

3. Methodology

The Dragonette-001 imagery was atmospherically corrected using ACOLITE's Dark Spectrum Fitting mode (Vanhellemont and Ruddick, 2018), to retrieve ρ_w. To reduce the impact of information leakage and spatial autocorrelation between training and testing datasets used for predictive modeling, a spatial blocking approach (Knudby and Richardson, 2023) was implemented to divide the samples into training (75%) and testing (25%) subsets. Specifically, a grid was superimposed over the study area, and random grid cells were progressively assigned to the test set until it contained at least 25% of the total samples, achieving an approximate 75:25 split. The grid cell size was defined as the semivariogram range of each WQP, ensuring statistical independence between neighbouring blocks.

A RF algorithm was used to estimate turbidity, SS, and DOC from ρ_w derived from Dragonette-001 imagery. Model development and training were implemented in Python using the *scikit-learn* library (Buitinck et al., 2013). RF was selected because it is easy to implement, allows interpretation of feature importance, and as an empirical approach, it can map non-optically active WQPs such as DOC. To improve model performance and prevent overfitting, key hyperparameters were optimized using the *Optuna* library (Akiba et al., 2019) with 5-fold cross-validation, which applies a Bayesian optimization strategy to explore the parameter space efficiently. During hyperparameter tuning, the following search ranges were used:

n_estimators between 50 and 2,000, *max_depth* between 3 and 200, *min_samples_split* between 2 and 70, *min_samples_leaf* between 1 and 70, and *max_features* selected from either "sqrt" or "log2". Model performance was evaluated using the RMSE, and maps of the three WQPs were produced for the acquisition dates of 2 August and 6 September 2024.

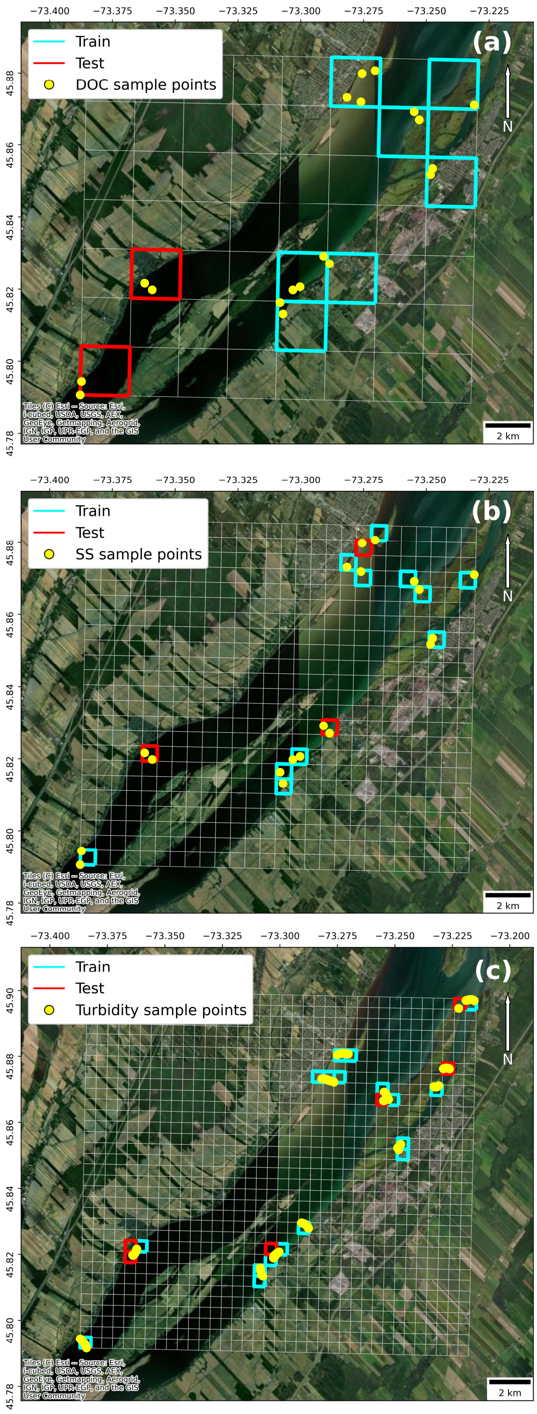

Figure 1. Study area on the St. Lawrence River with sampling points (yellow points) for (a) DOC, (b) SS, and (c) turbidity. Blue and red grid cells represent the training and testing subsets, respectively, for each WQP.

4. Results

4.1 Matchups

The distribution of training and testing samples for each parameter, along with the corresponding semivariogram ranges, is summarized in Table 1. The spatial blocking scheme is illustrated in Figure 1, while the corresponding semivariograms are shown in Figure 2. Due to random grid selection and unequal sample distribution within cells, the intended 75:25 split was not strictly achieved.

WQPs	DOC	SS	Turbidity
Semivariogram Range (m)	1,512	462	364
Training Samples	18	16	9,716
Testing Samples	3	5	2,520

Table 1. Sample distribution and semivariogram ranges.

Figure 3 shows ACOLITE outputs over the study area on 6 September 2024. To better characterize the spectral response of Dragonette-001 to WQPs, observations representing the minimum, median, and maximum values of each WQP were selected, and their corresponding ρ_w values were plotted across all spectral bands, with the resulting spectral signatures presented in Figure 4.

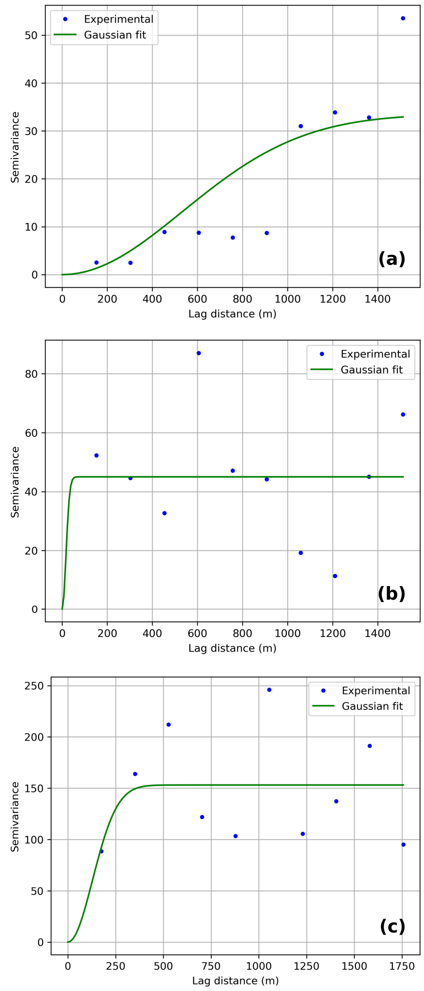

Figure 2. Semivariogram of (a) DOC, (b) SS, and (c) turbidity.

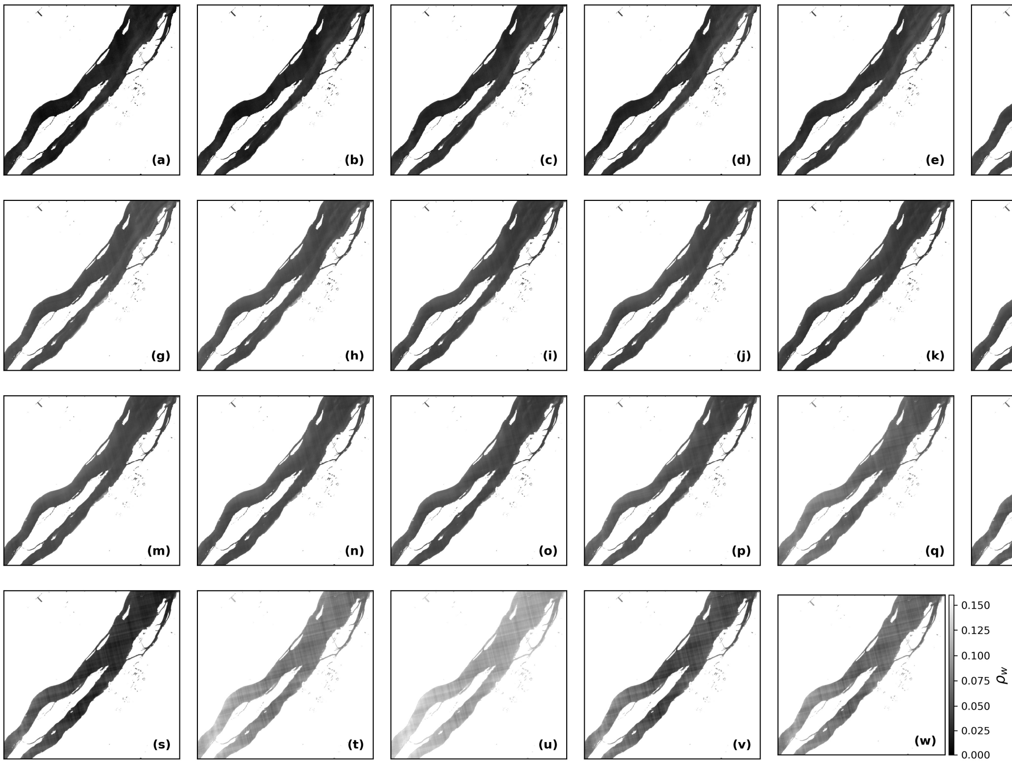

Figure 3. ACOLITE outputs for Dragonette-001 imagery over the study area on 6 September 2024. Panels correspond to the following spectral bands: (a) 503 nm, (b) 510 nm, (c) 519 nm, (d) 535 nm, (e) 549 nm, (f) 570 nm, (g) 584 nm, (h) 600 nm, (i) 614 nm, (j) 635 nm, (k) 649 nm, (l) 660 nm, (m) 669 nm, (n) 679 nm, (o) 690 nm, (p) 699 nm, (q) 711 nm, (r) 722 nm, (s) 734 nm, (t) 750 nm, (u) 764 nm, (v) 782 nm, and (w) 799 nm.

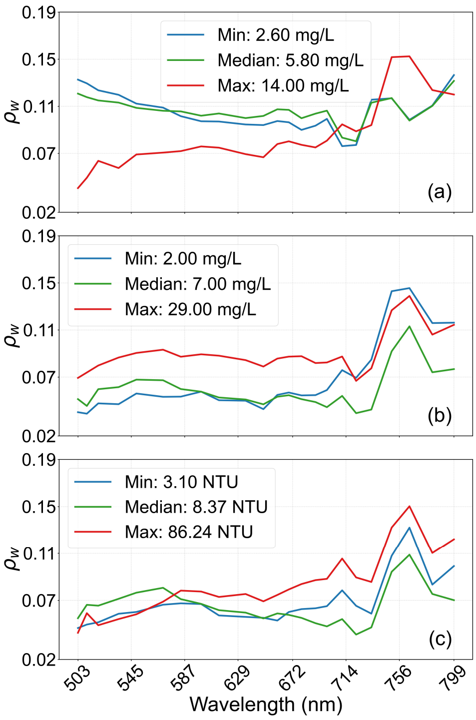

Figure 4. Spectral signatures corresponding to the selected observations representing minimum, median, and maximum values for each WQPs: (a) DOC, (b) SS, and (c) turbidity.

4.2 WQPs retrieval

Table 2 summarizes the optimized RF hyperparameters, while Figure 5 presents the feature importance of spectral bands for each parameter. Figure 6 presents scatter plots of observed versus predicted values for the testing dataset for each WQP, with the corresponding R^2 and RMSE values listed in Table 3. Figures 7 and 8 show the spatial maps of the three parameters for 2 August and 6 September 2024, respectively.

WQPs	DOC	SS	Turbidity
n_estimators	724	1,828	1,189
max_depth	119	136	134
min_samples_split	3	2	2
min_samples_leaf	1	1	1
max_features	log2	log2	log2

Table 2. Optimized RF hyperparameters using Optuna and 5-fold cross-validation for DOC, SS, and turbidity.

WQPs	DOC	SS	Turbidity
R^2	0.31	0.23	0.91
RMSE	2.83 (mg/L)	7.30 (mg/L)	3.63 (NTU)
Minimum	2.60 (mg/L)	2.00 (mg/L)	3.10 (NTU)
Median	5.80 (mg/L)	7.00 (mg/L)	8.37 (NTU)
Mean	6.14 (mg/L)	9.33 (mg/L)	13.85 (NTU)
Maximum	14.00 (mg/L)	29.00 (mg/L)	86.24 (NTU)

Table 3. Performance metrics of the RF models for DOC, SS, and turbidity, showing R^2 and RMSE values for the testing dataset, as well as the minimum, median, mean, and maximum values of the full dataset.

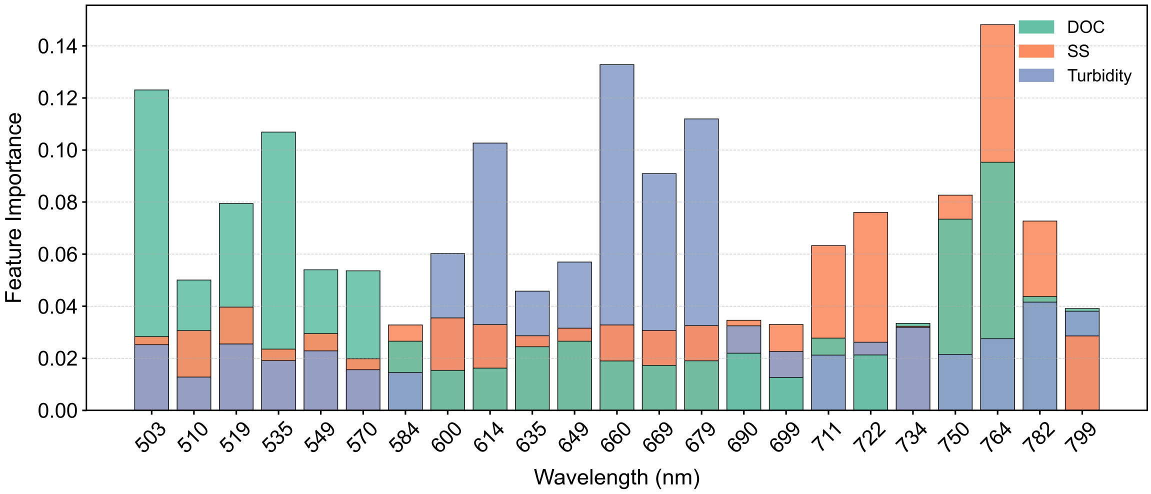

Figure 5. Feature importance of spectral bands for DOC, SS, and turbidity. All bars originate from the x-axis.

5. Discussion

Based on Figure 3, diagonal linear noise patterns are evident in the Wyvern Dragonette-001 imagery, particularly from 699 nm onwards (Figure 3 (p-w)). Given the high absorption coefficient of water in the NIR region, ρ_w in NIR bands is expected to be negligible (IOCCG, 2010; Mishra et al., 2017). However, as shown in Figures 3 (u) and 4, ρ_w at 764 nm exhibits relatively higher values compared to other bands. This elevated ρ_w in the NIR bands could be attributed to high turbidity, adjacency effects, potential limitations in ACOLITE's estimation of aerosol contributions, or possible issues specific to the sensor's NIR bands, including calibration inaccuracies or elevated noise. The especially high ρ_w at 764 nm is likely related to incorrect atmospheric correction near the O_2 absorption feature at ~762 nm. Notably, previous work (Ansari et al., 2025b) in a similar study area using Sentinel-2 imagery showed that reducing adjacency effects led to improved turbidity estimation, suggesting that adjacency effects may also play a role in the present results. Future studies with in-situ ρ_w measurements are recommended to determine whether these high values result from high turbidity, adjacency effects, ACOLITE, or issues in the Dragonette-001 NIR band.

Feature importance analysis using the RF model (Figure 5) shows that DOC retrieval relies primarily on six spectral bands in the green region: 503, 510, 519, 535, 549, and 570 nm. This observation aligns with Figure 4(a), where increasing DOC concentration corresponded to a decrease in ρ_w in these bands, suggesting a correlation between concentration of DOC and green-band ρ_w in Dragonette-001 imagery. For SS, the most important bands fall in the NIR region (Figure 5): 711, 722, 750, 764, and 782 nm. This observation does not align with Figure 4(b), where ρ_w for median SS concentration was lower than for minimum or maximum concentrations in these bands. Based on Figure 5, turbidity modeling relied on seven red bands (600, 614, 635, 649, 660, 669, and 679 nm), which is consistent with Figure 4(c), showing that ρ_w increased with turbidity in this spectral range.

Figure 6 shows that the turbidity model outperformed the DOC and SS models, likely due to the larger number of in-situ observations. For effective monitoring of turbidity and SS,

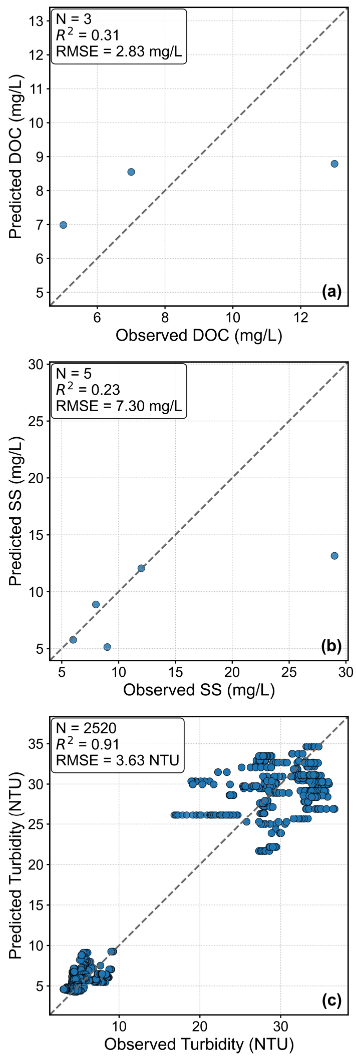

Figure 6. Scatter plots of observed versus predicted values for the testing dataset: (a) DOC, (b) SS, and (c) turbidity, with corresponding R² and RMSE value.

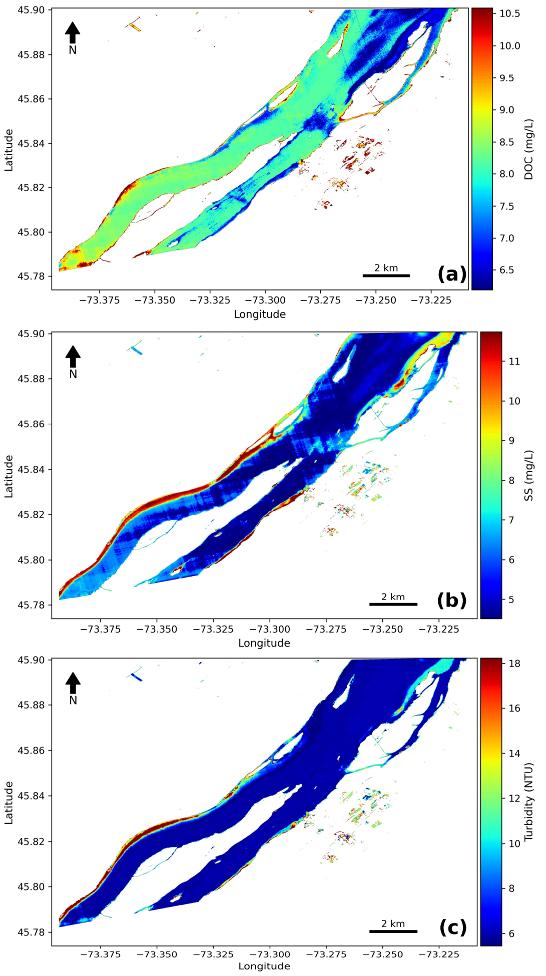

Figure 7. Spatial distribution maps of the WQPs estimated from Dragonette-001 imagery on 2 August 2024: (a) DOC, (b) SS, and (c) turbidity.

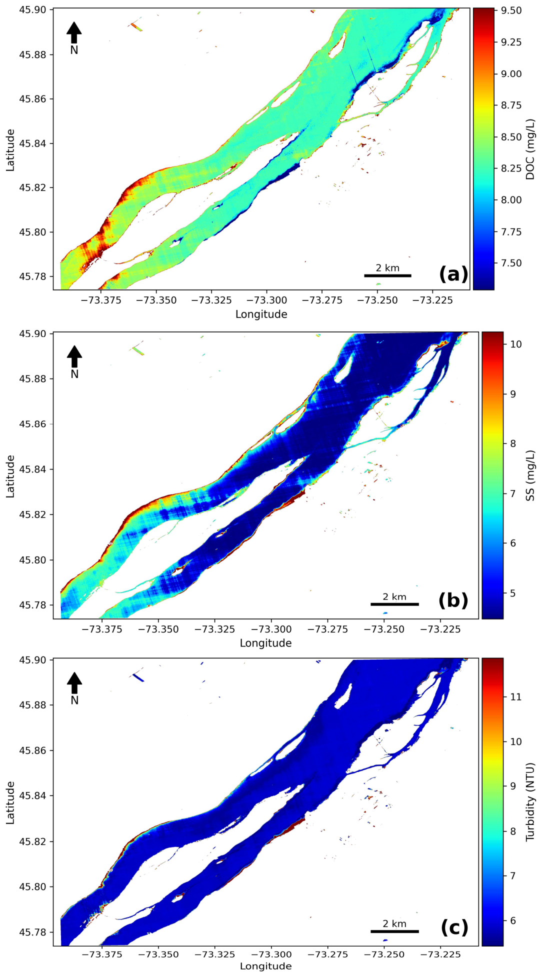

Figure 8. Spatial distribution maps of the WQPs estimated from Dragonette-001 imagery on 6 September 2024: (a) DOC, (b) SS, and (c) turbidity.

parameters closely associated with non-algal particles, two spectral regions are particularly informative: 475-640 nm and 710-775 nm (Ansari et al., 2025a; Mishra et al., 2017). The Dragonette-001 sensor covers 11 bands within the first range and 6 bands within the second, which likely contributed to its good performance in turbidity mapping.

Since only a fraction of DOC contributes to light absorption in the visible spectrum, the RF model mapped the optically active component of DOC, i.e., CDOM. Because CDOM and DOC are generally correlated, variations in total DOC can be partially inferred using CDOM as a proxy (Valerio et al., 2018). Accurate CDOM retrieval, however, typically requires blue-to-green bands (e.g., 380, 412, 425, 440 nm) (Ansari et al., 2025a; Mishra et al., 2017) that are absent in Dragonette-001, limiting the sensor’s ability to fully capture CDOM absorption features. Next-generation Dragonette sensors (e.g., Dragonette-002 and -003) with extended spectral coverage from 445-880 nm and 32 bands (Wyvern Dragonette, 2023) are expected to improve CDOM and DOC retrieval accuracy.

Overall, as shown in Table 3, RMSE values for all three WQPs are within acceptable ranges relative to the observed minimum and maximum values. Increasing the number of in-situ samples in future studies would further improve model reliability and strengthen conclusions about the sensor’s capability to map these WQPs.

Spatial maps (Figures 7 and 8) are consistent with field observations, showing higher turbidity, SS, and DOC values near the northern riverbank in compared to southern part. Turbidity maps (Figures 7(c) and 8(c)) appear smoother and less noisy than those for DOC or SS, likely reflecting better model performance. In SS maps (Figures 7(b) and 8(b)), diagonal linear noise patterns similar to those in the ρ_w imagery (Figure 3 (p-w)) are visible. These patterns are less pronounced in DOC and turbidity maps, likely because the RF model assigned higher feature importance to the NIR bands for SS, transferring linear band-specific noise to the final SS maps. In contrast, NIR bands were not among the most important for DOC or turbidity, reducing the impact of NIR band noise on their spatial outputs.

6. Conclusion

This study evaluated the feasibility of using Wyvern Dragonette-001 hyperspectral imagery for retrieving inland WQPs, including turbidity, SS, and DOC, in the St. Lawrence River. The results demonstrate that the sensor shows potential for mapping turbidity, which achieved high predictive performance ($R^2 = 0.91$) and produced spatially coherent maps consistent with field observations. The relatively lower performance observed for SS and DOC can be attributed, in part, to the limited number of in-situ samples available for SS and DOC, which constrained model training. In addition, linear noise present in the NIR bands, identified as important predictors for SS, appears to have propagated into the final maps. For DOC, the absence of blue spectral bands (<500 nm), which are critical for capturing CDOM absorption features, likely limited model performance, despite the ability of the empirical approach to partially infer DOC through its correlation with optically active components (e.g., CDOM).

The analysis also revealed challenges related to atmospheric correction. The unexpectedly high ρ_w values in NIR bands may be attributed to several factors, including incomplete removal of aerosol contributions by ACOLITE, adjacency effects, high turbidity conditions, or potential limitations in the Dragonette-001 sensor, particularly possible calibration uncertainties or elevated noise in its NIR bands. Further investigation, particularly using in-situ ρ_w measurements, is required to better distinguish between these possible sources.

Overall, the reported RMSE values are acceptable relative to the observed data ranges, supporting the potential of Dragonette-001 for practical WQP monitoring. However, increasing the number of in-situ samples, particularly for SS and DOC, would improve model robustness and reliability. Next Dragonette missions (e.g., Dragonette-002 and Dragonette-003) with extended spectral coverage are also expected to enhance the retrieval of WQPs such as CDOM and DOC.

In conclusion, this study shows that Dragonette-001 can be used for inland water quality monitoring, particularly for turbidity, while also highlighting limitations related to spectral coverage and atmospheric correction that should be considered in future applications.

7. Acknowledgements

The authors would like to acknowledge the Canadian Space Agency for the financial support under the smartHarbour initiative, implemented in collaboration with Public Services & Procurement Canada and the Montréal Port Authority to foster the development and adoption of best practices for environmental monitoring as well as the protection of terrestrial and aquatic ecosystems. Additional support was provided by WSP, the Mitacs Accelerate program (IT40023), and members of the University of Ottawa’s Shallow Water Earth Observation Laboratory. Assistance from ChatGPT-4o was used for portions of code development (e.g. code structure and debugging) and improving readability (e.g. text editing and word suggestions). All outputs were reviewed and edited by the authors as needed.

References

Akiba, T., Sano, S., Yanase, T., Ohta, T., Koyama, M., 2019. Optuna: A Next-generation Hyperparameter Optimization Framework, in: Proceedings of the 25th ACM SIGKDD International Conference on Knowledge Discovery & Data Mining, KDD ’19. Association for Computing Machinery, New York, NY, USA, pp. 2623–2631. https://doi.org/10.1145/3292500.3330701

Ansari, M., Knudby, A., Amani, M., Sawada, M., 2025a. Retrieving Inland Water Quality Parameters via Satellite Remote Sensing: Sensor Evaluation, Atmospheric Correc tion, and Machine Learning Approaches. Remote Sens. 17, 1734. https://doi.org/10.3390/rs17101734

Ansari, M., Wu, Y., Knudby, A., Ansari, M., Wu, Y., Knudby, A., 2025b. Assessing the Impact of T-Mart Adjacency Effect Correction on Turbidity Retrieval from Landsat 8/9 and Sentinel-2 Imagery (Case Study: St. Lawrence River, Canada). Remote Sens. 18. https://doi.org/10.3390/rs18010127

Buitinck, L., Louppe, G., Blondel, M., Pedregosa, F., Mueller, A., Grisel, O., Niculae, V., Prettenhofer, P., Gramfort, A., Grobler, J., Layton, R., Vanderplas, J., Joly, A., Holt, B., Varoquaux, G., 2013. API design for mach ine learning software: experiences from the scikit-learn project. https://doi.org/10.48550/arXiv.1309.0238

Gholizadeh, M.H., Melesse, A.M., Reddi, L., 2016. A Comprehensive Review on Water Quality Parameters Estimation Using Remote Sensing Techniques. Sensors 16, 1298. https://doi.org/10.3390/s16081298

IOCCG, 2010. Atmospheric Correction for Remotely-Sensed Ocean-Colour Products (No. 10), IOCCG Report Series. International Ocean Colour Coordinating Group, Dartmouth, Canada.

IOCCG, 2000. Remote Sensing of Ocean Colour in Coastal, and Other Optically-Complex, Waters (No. 3), IOCCG Report Series. International Ocean Colour Coordinating Group, Dartmouth, Canada.

Knudby, A., Richardson, G., 2023. Incorporation of neighborhood information improves performance of SDB models. Remote Sens. Appl. Soc. Environ. 32, 101033. https://doi.org/10.1016/j.rsase.2023.101033

Mishra, D.R., Ogashawara, I., Gitelson, A.A., 2017. Bio-optical Modeling and Remote Sensing of Inland Waters. Elsevier.

Tesfaye, A., 2024. Remote Sensing-Based Water Quality Parameters Retrieval Methods: A Review. East Afr. J. Environ. Nat. Resour. 7, 80–97. https://doi.org/10.37284/eajenr.7.1.1753

Valerio, A. de M., Kampel, M., Vantrepotte, V., Ward, N.D., Sawakuchi, H.O., Less, D.F.D.S., Neu, V., Cunha, A., Richey, J., 2018. Using CDOM optical properties for estimating DOC concentrations and pCO2 in the Lower Amazon River. Opt. Express 26, A657–A677. https://doi.org/10.1364/OE.26.00A657

Vanhellemont, Q., Ruddick, K., 2018. Atmospheric correction of metre-scale optical satellite data for inland and coastal water applications. Remote Sens. Environ. 216, 586–597. https://doi.org/10.1016/j.rse.2018.07.015

Wyvern Dragonette, 2023. Wyvern Dragonette Hyperspectral Satellites. Wyvern. URL https://wyvern.space/our-products/generation-one-hyperspectral-satellites/ (accessed 10.23.25).